Exchange Spin Coupling in Optically Excited States

Torben Steenbock[⋆,†], Lawrence L.M. Rybakowski[†], Dominik Benner[†],
Carmen Herrmann[†,‡], and Gabriel Bester[†,‡]

† Department of Chemistry, University of Hamburg, HARBOR, Building 610, Luruper
Chaussee 149, Hamburg, 22761 Germany.

‡ The Hamburg Centre for Ultrafast Imaging, Luruper Chaussee 149, Hamburg, 22761
Germany.

⋆ To whom correspondence should be addressed
email: torben.steenbock@chemie.uni-hamburg.de

Date: March 2nd, 2022

Status: Draft in final version

Abstract

In optically excited states in molecules and materials, coupling between local electron spins plays an important role for their photoemission properties and is interesting for potential applications in quantum information processing. Recently, it was experimentally demonstrated that the photogenerated local spins in donor–acceptor metal complexes can interact with the spin of an attached radical, resulting in a spin-coupling dependent mixing of excited doublet states, which controls the local spin density distributions on donor, acceptor, and radical subunits in optically excited states. In this work, we propose an energy-difference scheme to evaluate spin coupling in optically excited states, using unrestricted and spin-flip simplified time-dependent density functional theory (sTDDFT). We apply it to three platinum complexes which have been studied experimentally to validate our methodology. We find that all computed coupling constants are in excellent agreement with the experimental data. In addition, we show that the spin coupling between donor and acceptor in the optically excited state can be fine-tuned by replacing platinum with palladium and zinc in the structure. Besides the two previously discussed excited doublet states (one bright and one dark), our calculations reveal a third, bright excited doublet state which was not considered previously. This third state possesses the inverse spin polarization on donor and acceptor with respect to the previously studied bright doublet state and is by an order of magnitude brighter, which might be interesting for optically controlling local spin polarizations with potential applications in spin-only information transfer and manipulation of connected qubits.

1   Introduction

Exchange spin coupling in optically excited states is relevant for understanding and controlling the optical and magnetooptical properties in a variety of nanostructured systems ranging from molecules [1–4], nanoparticles [5,6], and quantum dots [7–9], to solids [10]. Nanoscopic systems in which spin coupling can be controlled by laser pulses [11,12] have potential applications in spin-only information transfer, storage [11,13], and quantum information processing [14–16]. While many studies have contributed to the understanding of spin coupling in the ground state, both theoretically [17–19] and experimentally [20,21], little is known on spin coupling in optically excited states [10].

A particularly interesting class of molecules showing spin coupling in optically excited states is based on donor–acceptor molecules substituted with radicals, where spins are created on the donor and acceptor subunits upon photoexcitation and subsequent charge transfer (see Figure 1) [16,22–25]. As for the electronic ground states, the phenomenological Heisenberg-Dirac-van Vleck (HDvV) Hamiltonian is usually employed for interpreting experimental data on the spin coupling in optically excited states [4,9],

$$\hat{H}_{\text{HDvV}} = \sum_{A<B} -2J_{AB}\hat{\mathbf{S}}_A\hat{\mathbf{S}}_B, \tag{1}$$

with J_{AB} referring to the spin coupling between the spins on different centers A and B, and $\hat{\mathbf{S}}_A/\hat{\mathbf{S}}_B$ being the corresponding local spin vector operators. The central quantity of interest is the exchange spin coupling constant, J_{AB}. Its magnitude descibes the strength and its sign the preferred kind of coupling between the spins, antiferromagnetic (antiparallel) or ferromagnetic (parallel).
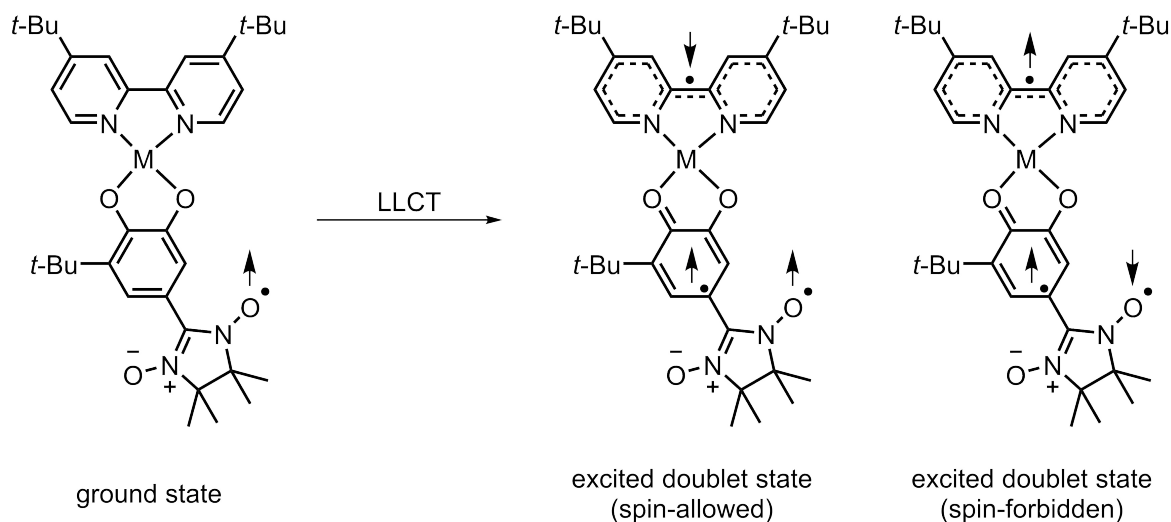
Figure 1: Example for the creation of local spins on donor and acceptor by photoexcitation: Ligand-to-Ligand-Charge-Transfer (LLCT) excited state in a (t-Bu$_2$bpy)M(Cat-NN) complex (Cat=3-tert-butyl-ortho-catecholate; bpy=bipyridine; NN=nitronyl-nitroxide; t-Bu=tert-butyl) and resulting excited doublet states (arrows in the structures represent the orientation of local spins on radical, donor and acceptor), as investigated experimentally in Ref. [4].

In order to understand spin coupling in optically excited states in such donor–acceptor complexes with radical substituents, much research effort has been dedicated to ground-state analogues of their charge-separated excited states [26–31]. Recently, Stein and coworkers [4] have investigated a series of (t-Bu$_2$bpy)Pt(Cat-R) (R=-NN, -ThNN, -PhNN; Cat=3-tert-butyl-ortho-catecholate; bpy=bipyridine; NN=nitronylnitroxide; Ph=phenyl; Th=thiophenyl) complexes (see Figure 2), for which they carried out low-temperature circular magnetic dichroism (CMD) measurements to extract spin coupling constants for optically excited states. They employed the HDvV Hamiltonian within an effective spin formalism to calculate the mixing between two photoexcited doublet states (for more details see Section 2.4 and Section S2 of the Supporting Information) [4,32]. This mixing depends on the spin coupling between donor and acceptor, and between donor and radical. Based on this mixing, they could also calculate the

4

spin populations on the donor, acceptor, and radical fragments that vary in their magnitude depending on the mixing strength. One of the excited doublet states taken into account by Stein and coworkers can be obtained from the doublet ground state (left part of Figure 1) by a spin-allowed (bright) charge-transfer (CT) excitation between the donor and the acceptor group, while a second one is a spin-forbidden (dark) excited CT state forming a local triplet state on the donor–acceptor fragment (right side of Figure 1). The remaining spin on the radical is then aligned with the photoexcited spins in such a fashion that global doublet states are obtained.
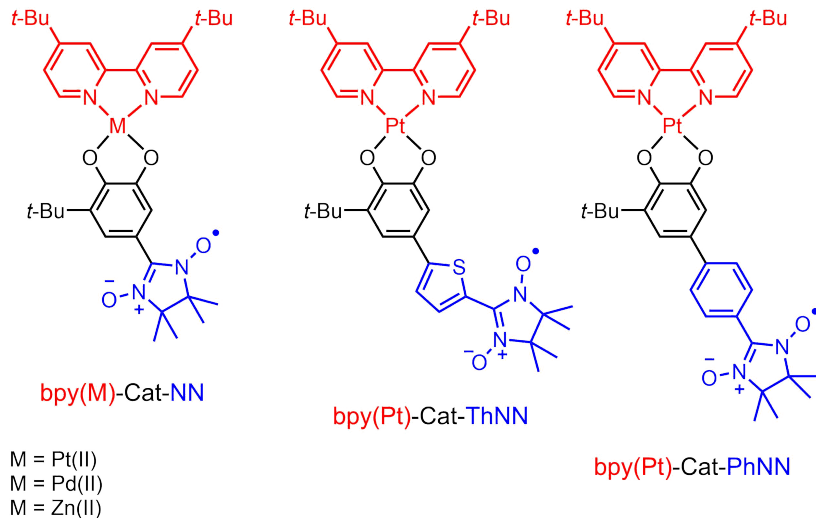
Figure 2: Five complexes under investigation in this work, consisting of bpy(M) acceptors (red), Cat donors (black), and NN radicals (blue) fragments. This chemical structures differ in the radical groups and in the metal centers.

Our first goal is to establish a methodology to calculate the excited states and spin coupling constants for optically excited states based on energy differences between excited-state energies computed with simplified time-dependent density functional theory (sTDDFT) [33]. We use sTDDFT in the unrestricted formalism [34] to calculate the spin-conserving (bright) doublet states and spin-flip sTDDFT (SF-sTDDFT) [35] for the dark excited doublet states. In a next step, we apply our methodology to a series of donor–acceptor–radical complexes (Figure 2). The Pt(II)-containing com-

pounds investigated experimentally by Stein and coworkers [4] give us the possibility to validate our methodology for calculating spin coupling constants. The Pd(II) and Zn(II) complexes were not studied experimentally yet and are taken into account as a potential way to fine-tune the spin coupling between the bpy(M) acceptors and the Cat donor. In the following, we will use the abbreviations for the different fragments introduced in Figure 2. We will refer to the red fragment as bpy(M) (with M=Pt(II), Pd(II), Zn(II); bpy=bis-tert-butyl-bipyridine), to the black fragment as Cat, and to the to blue fragment as R (with R= -NN, -ThNN, -PhNN; NN=nitronylnitroxide; Ph=phenyl; Th=thiophenyl).

Apart from the two excited doublet states mentioned in the work of Stein and coworkers [4] (Figure 1), we investigate a third bright (spin-allowed) charge-transfer excited doublet state which is a few thousand wavenumbers (few hundred meV) higher in energy with respect to the other two. This doublet state was not previously taken into account because it was not required for evaluating the spin coupling between donor and acceptor experimentally. However, this state might be of interest because it may differ in the local spin polarizations on donor, acceptor, and radical subunits with respect to the previously known bright doublet state. Further, it is an order of magnitude larger brighter (Section S6 in the Supporting Information) than the experimentally studied bright doublet state. This would offer the possibility to switch local spin polarizations with light. While the spin-coupling dependent spin polarizations on the subunits in the two excited doublets states in Figure 1 were calculated previously [4] from the experimental coupling constants based on the HDvV formalism [32], the spin polarization effects in the third excited doublet state have not been studied yet. This is done in this work by applying a Löwdin local spin analysis to the optically excited states obtained from sTDDFT which to the best of our knowledge has not been reported before. Further, we adress the spin polarization in the remaining two doublet states and compare them to those from the HDvV formalism [32] in order to see if doublet mixing and thus spin polarization effects are fully covered by our methodology.

2 Extracting Magnetic Properties from Excited-State Calculations

In this section, we discuss the qualitative nature of the optically excited spin states obtained with sTDDFT (Section 2.1), the calculation of Löwdin local spin polarizations for optically excited states (Section 2.2), and the spin coupling constants for optically excited states (Section 2.3). Finally, we discuss the spin coupling dependent mixing between doublet spin states in three-spin systems (Section 2.4).

2.1 Optically Excited Spin States

The scheme introduced here for evaluating excited-state spin coupling is applicable to any excited-state electronic-structure method such as TDDFT [36–38] and configuration interaction singles (CIS) [39,40]. Here, we discuss the excited spin states and which single-particle configurations are mainly contributing to these using SF-sTDDFT and unrestricted sTDDFT calculations. The sTDDFT approach was formulated based on TDDFT in the Tamm-Dancoff approximation (TDA) by neglecting the response of the exchange–correlation functional to the excitation, evaluating the two-electron integrals based on damped Coulomb interactions between charge density monopoles, and restricting the configuration space to a selected energy range (10 eV in this work) [33]. We use sTDDFT because the excited-state wavefunctions are constructed as linear combinations of excited Slater determinants, which allows for the construction of proper spin states in contrast to DFT [41–43]. Furthermore, we restrict ourselves to the magnetic properties of the lowest excited state being dominated by single-particle charge-transfer excitations from the Cat-centered highest occupied molecular orbital (HOMO) to the bpy(M)-centered lowest unoccupied molecular orbital (LUMO), for which we can directly compare with the experimental findings in Ref. [4].
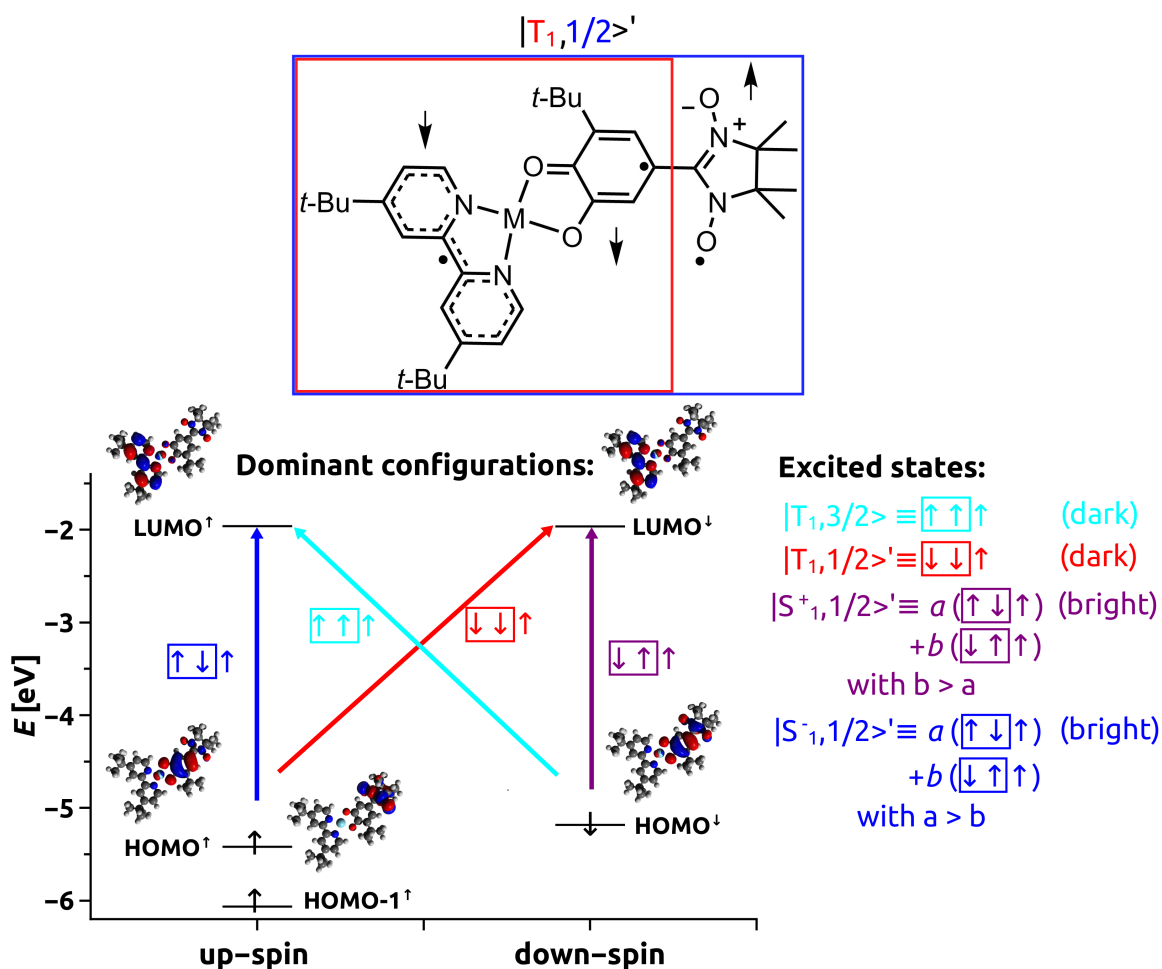
Figure 3: Frontier orbitals of the bpy(Pt)-Cat-NN donor-acceptor-radical system in the ground state obtained with CAM-B3LYP/def2-TZVP (bottom-left), dominant singly-excited spin configurations in the sTDDFT calculations (bottom-left). The arrows refer to the spins in the singly excited configurations (left arrow: bpy(M); middle arrow: Cat; right arrow: NN). The $\downarrow\downarrow\uparrow$ configuration possesses more down-spin than up-spin electrons because SF-sTDDFT is only implemented for spin-flip excitations from occupied up-spin to unoccupied down-spin MOs (being equivalent to $\uparrow\uparrow\downarrow$ in the absence of spin-orbit coupling) [35] and the excitation occurs from the doublet ground state with up-spin density (following the usual convention) on the radical group. The excited quartet and the three excited doublet states derived from these configurations are given on the right with the characterization as singlets and triplets being derived from the local spin configuration on the donor–acceptor subunit (red box in figure; T_1 referring to a parallel alignment of spins and S_1 to an antiparallel alignment of spin in the first excited spin-state manifold), and the number referring the total spin of the excited state (blue box in figure; 3/2 for quartet, and 1/2 for doublet).

Without loss of generality, we focus in this section on the MOs and excited states of the bpy(Pt)–Cat–NN system, because a qualitatively similar electronic structure is obtained for the remaining systems treated in this study (see Figures S1-S4 in the Supporting Information). Figure 3 shows the frontier orbitals (bottom-left) for up-spin and down-spin electrons calculated with the range-separated CAM-B3LYP functional [44] using Ahlrich's triple-zeta split-valence basis set with polarization functions on all atoms, def2-TZVP [45] (see Section 3). The HOMO-1$^\uparrow$ can be approximately identified as the singly occupied molecular orbital (SOMO; for the exact SOMO a corresponding orbital transformation is required [46]), carrying the spin in the ground state, which is mainly located on the NN subunit. For the bpy(Pt)–Cat–ThNN and the bpy(Pt)–Cat–PhNN system, the NN-located SOMOs constitute the HOMO-2$^\uparrow$ (Figure S1 and S2 in Supporting Information). The HOMOs in both spin orientations are located on the Cat, and the LUMOs on the bpy(M) subunits for all systems.

Starting from this electronic ground state, we performed sTDDFT calculations to obtain the different excited spin states arising from charge-transfer excitations between HOMOs and LUMOs. We do not take into account spin-orbit effects, so that transition to excited states obtained from SF-TDDFT possess no intensity in our calculations. The dominant singly-excited configurations contributing to these states are depicted with the colored arrows in Figure 3 (the exact weights of the dominant configurations are given in Figure 8 and discussed later). From these configurations, we can construct the different excited spin states: one quartet ($|T_1, 3/2\rangle$) and three doublet states ($|T_1, 1/2\rangle'$, $|S_1^+, 1/2\rangle'$, and $|S_1^-, 1/2\rangle'$). The notation employed here follows Ref. [4], and a similar notation was also used in Ref. [32]. T_1 (S_1) refers to the case where the local spins on the donor and acceptor are aligned parallel (antiparallel) in the first excited state, and the number refers to the spin of the total molecule in the excited spin state ($S=3/2$ for quartet and $S=1/2$ for doublet states). The prime used in the notation refers to doublet states mixed by spin coupling (while those without prime refer to the pure doublet states as discussed in Section 2.4). The plus and minus signs in $|S_1^+, 1/2\rangle'$ and $|S_1^-, 1/2\rangle'$ were introduced to distinguish the two doublet states

with local singlet configurations on the donor–acceptor fragment (and opposite sign of the local spin polarizations on donor and acceptor). The $\left|S_1^-, 1/2\right\rangle'$ excited doublet states addressed in this work were neglected in the work of Stein and coworkers [4]. The excited $\left|T_1, 1/2\right\rangle'$ and $\left|T_1, 3/2\right\rangle$ states can be constructed from spin-flip single-electron excitations and are mainly dominated by one configuration (cyan and red arrows in Figure 3). As a result, these states are spin-forbidden and dark. The bright $\left|S_1^+, 1/2\right\rangle'$ and $\left|S_1^-, 1/2\right\rangle'$ states obtained from spin-conserving, unrestricted sTDDFT calculations are dominated by two different configurations (depicted with blue and violet arrows in Figure 3). We find that the contributions of the $\uparrow\downarrow\uparrow$ and $\downarrow\uparrow\uparrow$ configurations to the bright $\left|S_1^+, 1/2\right\rangle'$ and $\left|S_1^-, 1/2\right\rangle'$ states are almost the opposite for both excited doublet states with the $\uparrow\downarrow\uparrow$ ($\downarrow\uparrow\uparrow$) configuration always being dominant for the $\left|S_1^-, 1/2\right\rangle'$ ($\left|S_1^+, 1/2\right\rangle'$) state (discussed in further detail in Section 4.2).

2.2 Löwdin local spin population analysis for excited states

To further analyze the local spins on the different fragments in the optically excited spin states from Section 2.1, we implemented and applied the Löwdin local spin analysis [47, 48] to excited states described by sTDDFT. This methodology can also be applied to similar excited-state electronic structure methods such as TDDFT and CIS, and was implemented into a development branch of the Artaios program package [49]. We chose Löwdin partitioning because the local projection operators can be properly defined compared to the pseudo projection operators used in the Mulliken population analysis [48, 50].

In analogy to the ground state, the local spin expectation values for a given atom (or fragment) A and excited state N, $\langle \hat{S}_{z,A}^N \rangle$, can be obtained as the sum over the differences between the corresponding elements of the density matrix in the Nth excited state for $\uparrow$ electrons, $\mathbf{D}^{\uparrow,N}$, and $\downarrow$ electrons, $\mathbf{D}^{\downarrow,N}$,

$$\langle \hat{S}_{z,A}^N \rangle = \frac{1}{2} \sum_{\mu \in A} \left(D_{\mu\mu}^{\uparrow,N} - D_{\mu\mu}^{\downarrow,N} \right), \tag{2}$$

10

where μ refers to a given atomic basis function in a symmetrically orthogonalized basis located on atom or fragment A (for details on Löwdin orthogonalization, see Section S1 in the Supporting Information). The elements of the density matrix can be calculated as the sum over all products of the corresponding elements of the occupation number vectors, $n_i^{\sigma,N}$, with the squared absolute values of the MO coefficients in the symmetrically orthogonalized basis, $c_{\mu i}^\sigma$,

$$D_{\mu\mu}^{\sigma,N} = \sum_i n_i^{\sigma,N} \left| c_{\mu i}^\sigma \right|^2, \tag{3}$$

with i being the index of the ith MO with spin σ. $\mathbf{n}^N$ is calculated by summing over all occupation number vectors for different configurations ja (ja referring to a single-particle excitation from occupied spin orbital j to an unoccupied spin orbital a), weighted by the absolute squared value of the sTDDFT amplitudes for a given configuration and excited state N, C_{ja}^N, obtained from the previous sTDDFT calculation,

$$\mathbf{n}^N = \sum_{ja} \left| C_{ja}^N \right|^2 \mathbf{n}_{ja}. \tag{4}$$

2.3 Exchange spin coupling in optically excited states

In this section, we discuss how the exchange spin coupling constants in an excited state can be calculated employing a HDvV Hamiltonian. All of the systems addressed in this work possess three spin centers in the optically excited charge-transfer state (see Figure 3). Under the assumption that the spins on the bpy(M) center and on the NN group do not interact, the HDvV Hamiltonian includes the spin coupling between the spins on the bpy(M) and on the Cat subunits, $J_{\text{bpy(M)-Cat}}$, and between the spins on the Cat and on the NN subunits, $J_{\text{Cat-NN}}$,

$$\hat{H}_{\text{HDvV}} = -2J_{\text{bpy(M)-Cat}}\hat{\mathbf{S}}_{\text{bpy(M)}}\hat{\mathbf{S}}_{\text{Cat}} - 2J_{\text{Cat-NN}}\hat{\mathbf{S}}_{\text{Cat}}\hat{\mathbf{S}}_{\text{NN}}. \tag{5}$$

Applying the strategy developed by Ruiz and coworkers [51], who extended the energy-difference method orginally proposed for two spin centers [41] to systems with three

or more spin centers, we obtain equations for the coupling constants in Equation (5). While Ruiz *et al.* employed ground-state energies, we employ the excited-state energies of the states discussed in Figure 3. As in the work of Ruiz and coworkers [51], we assumed ideal spins of $S = 1/2$ for all three spin centers to simplify the linear equations. With this, we obtain the following expressions for $J_{\text{bpy(M)-Cat}}$ and $J_{\text{Cat-R}}$ (the full derivation is given in Section S7 of the SI):

$$J_{\text{bpy(M)-Cat}} = \frac{E^{\left|S_1^+, 1/2\right\rangle'} - E^{\left|T_1, 3/2\right\rangle}}{2},$$ (6)

$$J_{\text{Cat-R}} = \frac{E^{\left|T_1, 1/2\right\rangle'} - E^{\left|T_1, 3/2\right\rangle}}{2},$$ (7)

As we deal with non-symmetric systems in this work, the linear equation system is overdetermined (see Ref. [51]), implying that the coupling constants are not uniquely determined by Equations (6) and (7) but also two alternative equations can be obtained also depending solely on the energies of the three doublet states (Section S7 in the SI). However, the experimental $J_{\text{bpy(Pt)-Cat}}$ was evaluated based on the energy difference between the $\left|T_1, 1/2\right\rangle'$ and $\left|S_1^+, 1/2\right\rangle'$ states in the MCD measurements [4] and the $\left|S_1^-, 1/2\right\rangle'$ state was not addressed. To be consistent with experiment, we will employ Equations (6) and (7) which only depend on the energies of the doublet states adressed in experiment.

2.4 Spin-coupling dependent mixing of excited doublet states

As already mentioned in the introduction, pure doublet states in three-spin systems can undergo a mixing induced by spin coupling which was described in detail within a HDvV formalism by Bencini *et al.* [32]. The mixing strength (defined in Equation (10)) for doublet states can be obtained by setting up the HDvV Hamiltonian matrix in the basis of the pure doublet states and then diagonalizing it to obtain the eigenvectors and eigenvalues. More details on the derivation of the mixing strength is given in Section SI2 in the Supporting Information, and the full derivation is given in Ref. [32]. Further, it

is possible to derive expressions for the local spins on acceptor, donor and radical for the optically excited states within the HDvV model solely depending on the mixing strength (Equations (14)–(22) in Section S3 of the Supporting Information). Bencini *et al.* took into account a three-spin system with two pure doublet states in the absence of mixing, $|S_1, 1/2\rangle$ and $|T_1, 1/2\rangle$. $|S_1, 1/2\rangle$ is replaced by $|S_1^+, 1/2\rangle$ and $|S_1^-, 1/2\rangle$ in this work, which according to the HDvV formalism both only possess local spins on the R unit in optically excited states when no mixing occurs (bottom left in Figure 4), which is the case if $J_{\text{bpy(M)-Cat}}$ is much larger than $J_{\text{Cat-R}}$. For the pure $|T_1, 1/2\rangle$ doublet state (bottom left in Figure 4), we expect the spins on the bpy(M) and Cat fragments to be aligned parallel, while the local spin on the R subunit is antiparallel to the other two (with a smaller magnitude). These pure doublet states start to mix when exchange spin coupling between the spins is considered. After setting up and diagonalizing the HDvV Hamiltonian matrix, the eigenvectors represent the mixed doublet states ($|S_1, 1/2\rangle'$ and $|T_1, 1/2\rangle'$; $|S_1, 1/2\rangle'$ stands for $|S_1^+, 1/2\rangle'$ and $|S_1^-, 1/2\rangle'$) in the basis of the pure doublet states,

$$|S_1, 1/2\rangle' = \cos(\lambda)|S_1, 1/2\rangle - \sin(\lambda)|T_1, 1/2\rangle, \tag{8}$$

$$|T_1, 1/2\rangle' = \cos(\lambda)|T_1, 1/2\rangle + \sin(\lambda)|S_1, 1/2\rangle, \tag{9}$$

with λ being the mixing strength between the doublet states that depends on the spin coupling constants $J_{\text{Cat-R}}$ and $J_{\text{bpy(M)-Cat}}$ (under the assumption that there is no spin coupling between the bpy(M) acceptor and R radical groups) [32],

$$\lambda = \frac{1}{2}\tan^{-1}\frac{\sqrt{3}J_{\text{Cat-R}}}{2J_{\text{bpy(M)-Cat}} - J_{\text{Cat-R}}}. \tag{10}$$

λ can take values beetween $0°$ and $30°$. The mixing strength itself increases almost linearly with increasing ratio between $J_{\text{Cat-R}}$ and $J_{\text{bpy(M)-Cat}}$ (top of Figure 4).

13
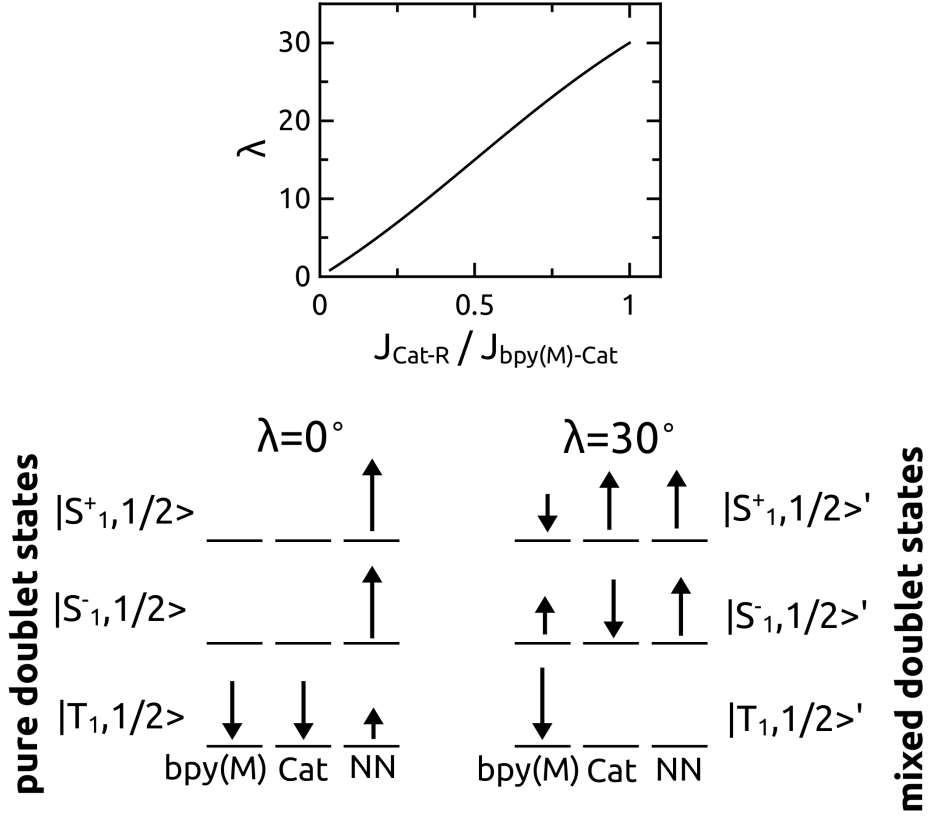
Figure 4: Doublet mixing strength λ as a function of the the ratio between $J_{\text{Cat-R}}$ and $J_{\text{bpy(M)-Cat}}$ (top) and local spins of the pure doublet states ($\lambda = 0°$; bottom-left) and the mixed doublet states in the strong mixing limit ($\lambda = 30°$; bottom-right) obtained from the HDvV formalism as a function of λ (Equations (14)–(22) in the Supporting Information).

For the maximal λ (30°), the mixed, bright doublet states ($|S_1^+, 1/2\rangle'$ and $|S_1^-, 1/2\rangle$) both show local spin polarization on the bpy(M) and Cat groups (with opposing sign; see Section S3 in the Supporting Information for further details), which was absent in the pure doublet states. For the dark $|T_1, 1/2\rangle'$ state in the strong mixing limit (when $J_{\text{Cat-R}}$ approaches $J_{\text{bpy(M)-Cat}}$), the local spins on the Cat and R groups vanish, and the only spin polarization remains on the bpy(M) fragment. The local spins obtained by Bencini *et al.* are later compared with the local spins obtained from our Löwdin local

14

spin analysis based on sTDDFT (Section 4.2).

3   Computational methodology

All molecular structure optimizations were carried out with the TURBOMOLE 7.4.1 program package [52] for the doublet ground state using Ahlrich's triple-zeta basis set with polarization functions on all atoms, def2-TZVP [45] (and employing effective core potentials for platinum and palladium to take into account scalar-relativistic effects), and the PBE exchange-correlation functional [53–56]. In these calculations, convergence criteria of $1\text{x}10^{-4}$ a.u. for the gradient and $1\text{x}10^{-7}$ hartree for the energy in the self-consistent-field algorithm were employed. On top of the optimized structures, single-point calculations with the range-separated hybrid functional CAM-B3LYP [44] and the def2-TZVP basis set were performed with the same convergence criteria. The CAM-B3LYP functional was employed because it is known to perform well for charge-transfer excited states [57] and also provides reasonable results for spin coupling in organic radicals in electronic ground states [58]. Finally, we carried out unrestricted sTDDFT [34] and SF-sTDDFT [35] calculations with the open-source STDA code by Grimme and coworkers [33] to obtain the excited spin states used for the calculation of the excited-state local spins and exchange coupling constants employing the parameters for CAM-B3LYP published in Ref. [59]. In this calculation we took all configurations up to an energy of 10 eV. Because SF-TDDFT is only implemented for spin-flip excitations occuring from occupied up-spin to down-spin MOs, we interchanged the converged up-spin and down-spin TURBOMOLE orbital files after the DFT calculation and then carried out an SF-sTDDFT calculation in order to obtain the optically excited quartet high-spin excited state. The coupling constants were then calculated by Equations (6) and (7), and the Löwdin local spins for the different excited states were evaluated with our in-house implementation of the Löwdin local spin population analysis for optically excited states (see Section 2.2) in a development version of the ARTAIOS program package [49] (available upon request), using the sTDDFT amplitudes obtained with

the sTDA program package.

4   Results and Discussion

In Section 4.1, we validate the methodology for calculating excited-state exchange coupling constants (Section 2.3) by applying it to the systems in Figure 2. We compare our results for the Pt(II) complexes with experimental values obtained from circular magnetic dichroism (CMD) measurements and magnetic measurements on ground state radical analogues of the excited, charge-separated states [4]. Moreover, we explore the possibilities of fine-tuning the exchange spin coupling between donor and acceptor by substituting Pt(II) with Pd(II) and Zn(II) in the complexes. In Section 4.2, we use the HDvV formalism to calculate the mixing strengths between the excited doublet states (see Section 2.4) based on the coupling constants obtained with our methodology and study the Löwdin local spins on acceptor, donor and radical groups for the different structures. Further, we compare these Löwdin local spins with those obtained from the HDvV formalism, where the local spins are a function of the mixing strength only (see Section S3 of Supporting Information), to see if all spin polarization appearing in HDvV formalism are recovered by our sTDDFT calculations.

4.1   Excited State Energies and Exchange Spin Coupling

In order to understand how the chemical structure of the radical groups (R) and the transition-metal substitution affect the energy splittings between the excited quartet and doublet states, these splittings are given in Figure 5 (excited-state energies oscillator strengths are available in Table S2 in the SI). For all systems, the same qualitative order of excited spin states is found. The lowest excited state is the $|T_1, 3/2\rangle$ quartet state, followed by three doublet states in the following energetic order: $\left|S_1^+, 1/2\right\rangle' < \left|T_1, 1/2\right\rangle' < \left|S_1^-, 1/2\right\rangle'$. The splitting between the $\left|S_1^+, 1/2\right\rangle'$ and the quartet state is

16

modified by the choice of the R radical group, but not by the choice of the metal center. On the other hand, the energetic difference between the $\left|S_1^+, 1/2\right\rangle'$ and $\left|T_1, 1/2\right\rangle'$ doublet states is only sensitive to the substitution of the metal center and increases from Pt(II) over Pd(II) to Zn(II), but not to the choice of the metal center.
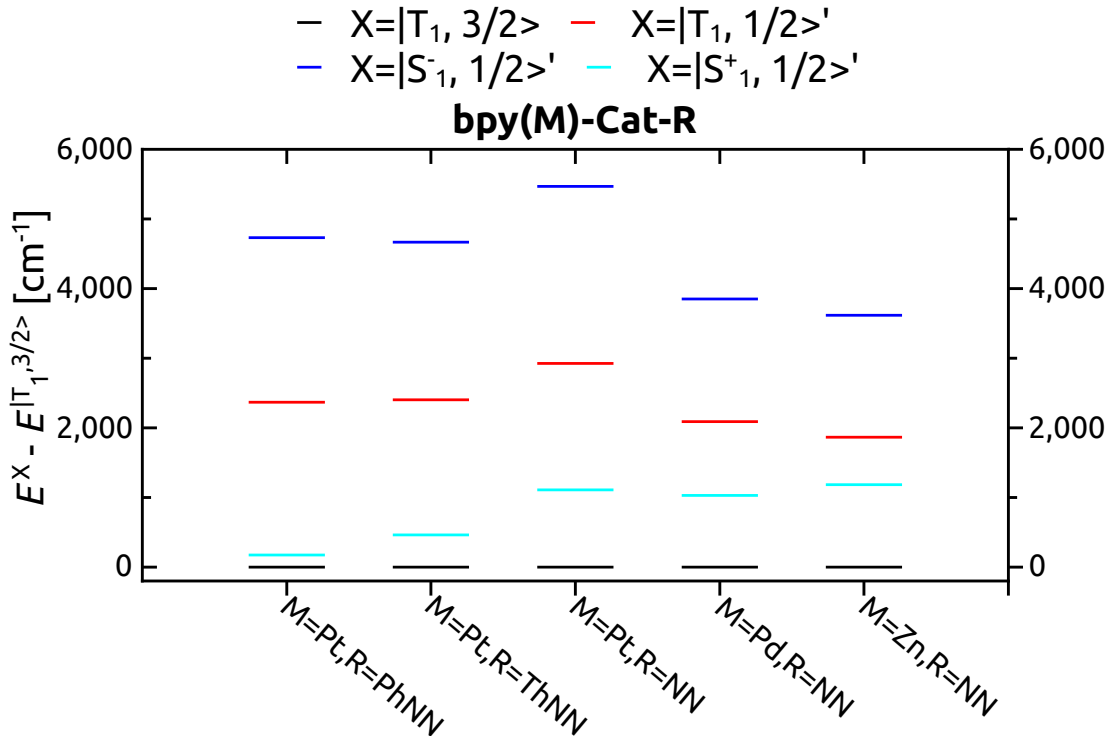
Figure 5: Excited-state energy splittings from sTDDFT for the quartet state and the three doublet states. All energies are referenced to the energy of the quartet state.

The trends in the energy differences are reflected in the exchange coupling constants from the excited-state energies employing Equations (6) and (7). The coupling constants are given in Figure 6 along with the experimental coupling constants obtained by Stein and coworkers [4] for comparison. The experimental $J_{\text{bpy(Pt)-Cat}}$ values were obtained from low-temperature circular magnetic dichroism (CMD) measurements on the $\left|T_1, 1/2\right\rangle'$ and $\left|S_1^+, 1/2\right\rangle'$ states of the bpy(Pt)-Cat-NN complex. The experimental $J_{\text{Cat-R}}$ coupling constants were taken from magnetic susceptibility measurements on

17

corresponding ground-state Cat-NN diradical analogues.
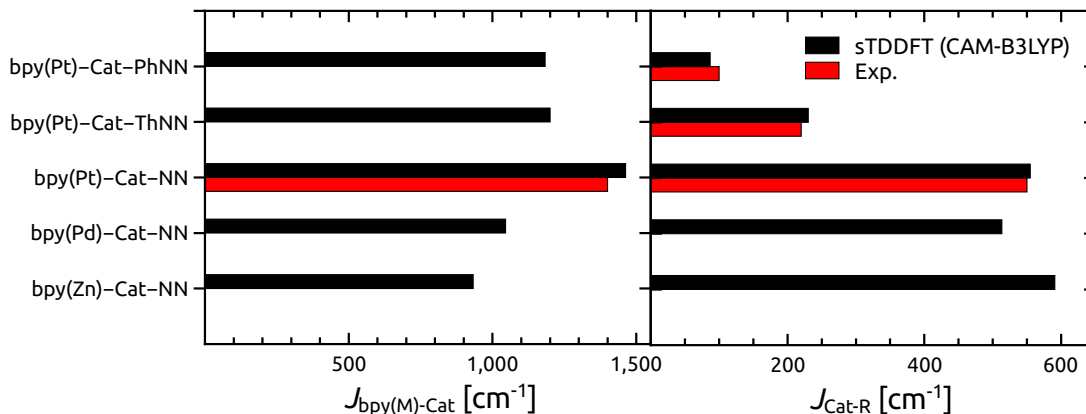
Figure 6: Excited-state spin coupling constants between the bpy(M) acceptor and the Cat donor (left panel), $J_{\text{bpy(M)-Cat}}$, and Cat donor and R (R=NN, ThNN, PhNN) radical (right panel), $J_{\text{Cat-R}}$, calculated with Equations (6), and (7), along with the experimental values from Ref. [4].

We find that all calculated coupling constants within this work are ferromagnetic and in quantitative agreement with the experimental values. It should be noted that Stein and coworkers assumed that the spin coupling constants between the Cat donor and bpy(Pt) acceptor ($J_{\text{bpy(M)-Cat}}$; left panel in Figure 6) are the same for all three experimentally investigated systems (bpy(Pt)-Cat-NN, bpy(Pt)-Cat-ThNN, and bpy(Pt)-Cat-PhNN), which is why only the coupling constant for the bpy(Pt)–Cat–NN complex was extracted from the CMD measurement. In our calculations, the $J_{\text{bpy(M)-Cat}}$ values for bpy(Pt)-Cat-ThNN and bpy(Pt)-Cat-PhNN (1200 cm^{-1} and 1183 cm^{-1}) are approximately 250 cm^{-1} lower than that of the bpy(Pt)-Cat-NN system (1463 cm^{-1}), which might be due to the HOMOs being delocalized onto the thiophene and phenyl rings in the former structures (see Figure S1-S2 in the Supporting Information). This delocalization might lead to an increase in the effective distance between the spins, and thus to a lower spin coupling strength. The replacement of Pt(II) in the bpy(Pt)-Cat-NN complex by Pd(II) and Zn(II) leads to a pronounced reduction of the spin coupling

18

between the bpy(M) and the Cat subunits, which can be rationalized by a decreasing overlap between the Cat- and bpy(M)-centered MOs on the metal center. This suggests an effective strategy for fine-tuning the spin coupling between the Cat and bpy(M) spin centers (Figure 6). The spin coupling constants between the Cat donor and the R (R=ThNN, PhNN, and NN) radical subunits, $J_{\text{Cat-R}}$, are also in good quantitative agreement with those from experiment [4]. $J_{\text{Cat–R}}$ decreases as a function of the radical group R in the following order: NN > ThNN > PhNN. This is in line with the strongly decreasing energy difference between the $\left|S_1^+, 1/2\right\rangle'$ doublet state and the quartet state in Figure 5. The changes in $J_{\text{Cat-R}}$ for different metal centers are insignificant because the metal center is located between the Cat and bpy ligand, not between the Cat and R subunit.

4.2 Mixing strengths and local spin properties

Due to the quantitative agreement of the theoretical coupling constants with experiment, also the doublet mixing strengths, λ, calculated from their ratio according to Equation (10) reproduce the experiment [4] well (top-left in Figure 7). The doublet mixing strengths increase from PhNN over ThNN to NN for the Pt(II) complexes and also increase for the bpy(M)-Cat-NN radicals when Pt(II) is replaced by Pd(II) and Zn(II). Both trends can be explained by the fact that the two spin coupling constants become more similar in magnitude. When changing the radical substituent R, the spin coupling between the R and the Cat subunit, $J_{\text{Cat-R}}$, is increased along the sequence, while the $J_{\text{bpy(M)-Cat}}$ coupling constants barely change. By contrast, replacing Pt(II) by Pd(II) and Zn(II) reduces the coupling constant $J_{\text{bpy(M)-Cat}}$, while $J_{\text{Cat-R}}$ is only slightly affected.
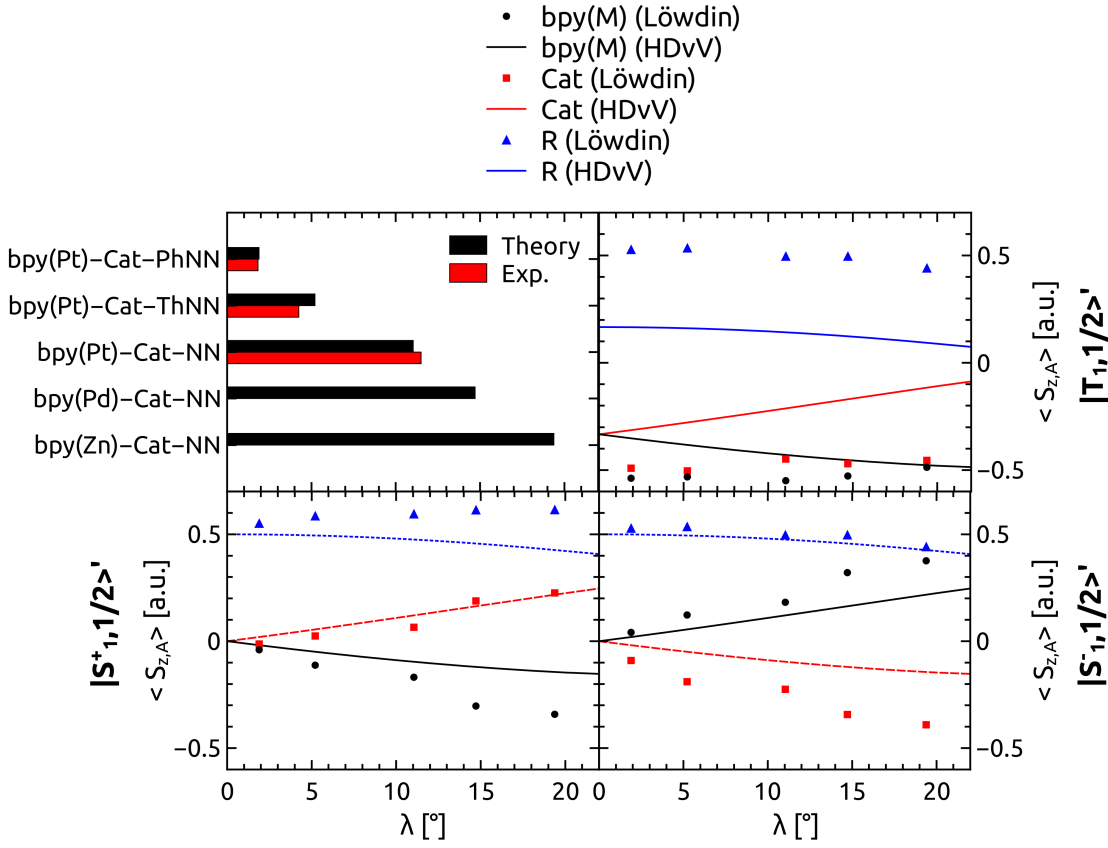
Figure 7: Calculated mixing strengths (λ) for the systems under investigation evaluated according to Equation (10) along with λ values taken from Ref. [4] (top-left). Local spins on the three spin centers calculated for doublet states with different mixing strengths λ: $|T_1, 1/2\rangle'$ (top-right), $|S_1^+, 1/2\rangle'$ (bottom-left), and $|S_1^-, 1/2\rangle'$ (bottom-right). The lines refer to the local spins from the HDvV formalism, which constitute λ-dependent functions (Equations (S14)-(S20) in Supporting Information). The dots refer to values from the Löwdin population analysis (Equation (2)) plotted against the corresponding λ parameter calculated according to Equation (10) from the theoretical coupling constants (Equations (6)-(7)).

In a next step, we calculated the Löwdin local spins for the three fragments as defined in Figure 2 and plotted them together with those obtained from the HDvV formalism (see Section S2 and S3 in the Supporting Information) for the three different doublet states:

$|\mathrm{T}_1, 1/2\rangle'$ (top-right in Figure 7), $\left|\mathrm{S}_1^+, 1/2\right\rangle'$ (bottom-left in Figure 7), and $\left|\mathrm{S}_1^-, 1/2\right\rangle'$ (bottom-left in Figure 7) as a function of the doublet mixing strength, λ, evaluated according to Equation (10). The magnitudes of the local spins for $\left|\mathrm{S}_1^+, 1/2\right\rangle'$ and $\left|\mathrm{S}_1^-, 1/2\right\rangle'$ on the bpy(M) (black dots) and Cat groups (red squares) strongly increase with increasing doublet mixing strength and have opposite signs, while the local spins on the R group (blue triangles) remain rather constant, in agreement with their "arrow" definitions in Figure 3. While the trends for the local spins on the bpy(M) and Cat fragments are qualitatively similar to the λ-dependent values from the HDvV model (red and black lines), we find that the local spins on the R group obtained from both approaches differ for the $\left|\mathrm{S}_1^+, 1/2\right\rangle'$ excited state (blue line and triangles; bottom-left in Figure 7). This difference might be explained by the fact that the Cat-centered MOs show contributions on the R group (see Section S4), and therefore up-spin is transferred from the Cat groups to the R groups $\left|\mathrm{S}_1^+, 1/2\right\rangle'$, increasing the local spin-up density on the R fragment. Such a behavior is not covered by the underlying HDvV Hamiltonian, which assumes rotations of perfectly localized spins and does not take into account changes of the spins' magnitudes due to delocalization onto neighboring spin centers [60, 61]. For the $|\mathrm{T}_1, 1/2\rangle'$ excited doublet state, the Löwdin local spins (top-right in Figure 7) are not affected much by increasing λ, which is in disagreement with the local spins from the HDvV formalism. According to the HDvV formalism, the local spins' magnitudes for the R and Cat fragments are expected to decrease and the local spins on the bpy(M) fragment should increase as a function of λ.

21
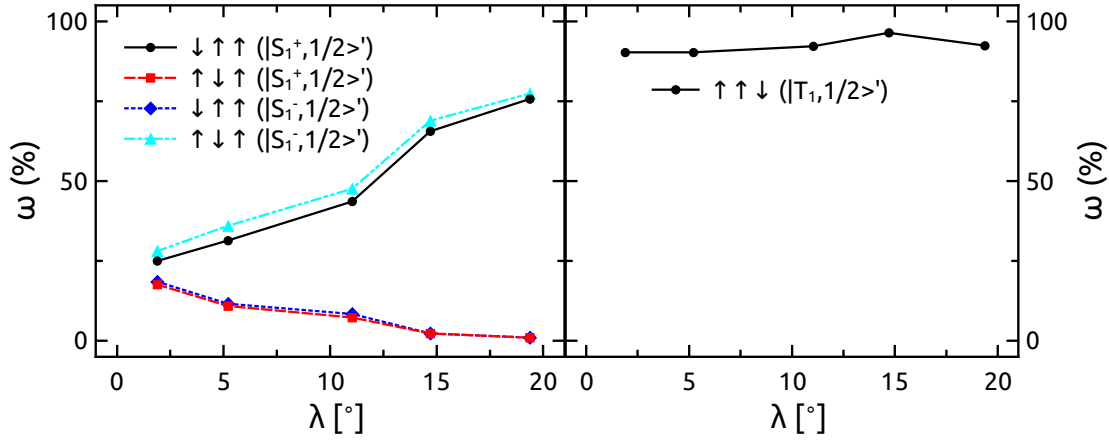
Figure 8: Most dominant contributions of single-particle configurations ω (for further details see Section 2.1) for the three excited doublet states: $\left|S_1^+, 1/2\right\rangle'$ (left; optically bright), $\left|S_1^-, 1/2\right\rangle'$, (left; optically bright) and $\left|T_1, 1/2\right\rangle'$ (right; optically dark) for the different systems represented by their λ values given in Figure 7).

In order to rationalize the differences between the HDvV formalism and the Löwdin local spins for the $\left|T_1, 1/2\right\rangle'$ state and to gain further insight into the trends for $\left|S_1^+, 1/2\right\rangle'$ and $\left|S_1^-, 1/2\right\rangle'$, we investigated the most dominant contributions from different singly-excited configurations to these excited states (Figure 8; for details on the definition of configurations see Section 2.1). For the bright doublet states ($\left|S_1^+, 1/2\right\rangle'$ and $\left|S_1^-, 1/2\right\rangle'$) we see that the ↓↑↑ (black and blue lines) and ↑↓↑ configurations (red and cyan lines) contribute almost equally to the excited states for small values of λ. The $\left|S_1^+, 1/2\right\rangle'$ ($\left|S_1^-, 1/2\right\rangle'$) excited doublet state is dominated by the ↓↑↑ (↑↓↑) configuration, and this domination continues to grow with increasing λ. These massive changes in the configuration contributions are in line with the λ-dependent Löwdin local spin polarization effects observed for $\left|S_1^+, 1/2\right\rangle'$ and $\left|S_1^-, 1/2\right\rangle'$ (Figure 8). The dark $\left|T_1, 1/2\right\rangle'$ excited state is solely dominated by the spin-flip ↓↓↑ configuration (right side of Figure 8), which only slightly changes as a function of λ. These small changes in the contributions can explain the rather constant local spin polarizations for $\left|T_1, 1/2\right\rangle'$ in Figure 7. The deviations between the HDvV formalism and the local Löwdin spin analysis for the

$|T_1, 1/2\rangle'$ state cannot be explained by erroneous coupling constants (energetics), since these are in excellent agreement with the experimental values. Moreover, problems with the Löwdin local spin analysis itself can be ruled out as the local spins obtained from both approaches agree well with each other for $|S_1^+, 1/2\rangle'$ and $|S_1^-, 1/2\rangle'$. edThe problem could potentially be related to the excited-state electronic structure method employed. A problem might be that the spin-flip and spin-conserving singly excited configurations are not treated simultaneously in one calculation, which appears not to influence the energetics much but the local spin properties.

5 Conclusion

In this work, we established a methodology to calculate spin coupling constants from excited-state energies employing spin-flip simplified time-dependent density functional theory (sTDDFT) and unrestricted sTDDFT for a series of bpy(M)–Cat–R donor–acceptor–radical complexes in the lowest LLCT excited state and compared them with previously published, experimental values [4]. With this methodology, we explore the possibility to fine-tune exchange spin coupling between the bpy(M) acceptor and the Cat donor by going beyond the experimentally known structures replacing Pt(II) with Pd(II), and Zn(II). We also adressed a third doublet state not discussed in previous work that, like the known doublet states, originates from linear combinations of the HOMO$^{\uparrow/\downarrow}$ to LUMO$^{\uparrow/\downarrow}$ excitations. This spin state is brighter than the previously studied, bright doublet state and shows inverse spin polarizations on donor and acceptor with respect to the known bright doublet state, which raises the possibility to optically control local spin polarizations.

We found that the coupling constants calculated are in excellent agreement with those from experiment [4] (Section 4.1), showing a decrease of spin coupling between Cat donor and radical group R from R=NN over R=ThNN to R=PhNN. The substitution of Pt(II) by Pd(II) and Zn(II) systematically reduces the strength of spin coupling

23

between the bpy(M) acceptor and the Cat donor. The mixing strengths between the excited doublet states from the exchange coupling constants employing the HDvV formalism [32] were also in quantitative agreement with the values from literature [4] (Section 4.2). The reduction of the spin coupling between donor and acceptor by metal substitution leads to a stronger mixing between the doublet states for the Zn(II) and Pd(II) compounds compared to the Pt(II) complexes. The third, previously not discussed (bright) excited doublet state $(\left|S_1^+, 1/2\right\rangle')$ possesses an inverse spin polarization with respect to the other bright excited doublet state $\left|S_1^-, 1/2\right\rangle$ on the bpy(M) acceptor and Cat donor groups (Section 4.2). We find that the Löwdin local spins obtained for the $\left|S_1^+, 1/2\right\rangle'$ and $\left|S_1^-, 1/2\right\rangle'$ states are in agreement with the spin-coupling dependent local spins obtained from the HDvV formalism [32]. For the $\left|T_1, 1/2\right\rangle'$ state, we find larger deviations between the HDvV formalism and the Löwdin local spins, which might be explained by the fact that in SF-sTDDFT, only spin-flip singly excited configurations enter the calculation. This limitation could be overcome by employing a more generalized approch including both types of configurations, spin-flipped and spin-conserving, in one calculation, such as in the windowed Full-CI approach used by Pfäffle and coworkers [62]. Moreover, to consider the effects of the doublet mixing on the intensities and on the lifetimes of formally spin-forbidden excited states, it might be of interest to apply a quasirelativistic, two-component DFT approach in future work. From the experimental point of view, the inverse local spin polarizations on donor and acceptor in the $\left|S_1^+, 1/2\right\rangle'$ and $\left|S_1^-, 1/2\right\rangle$ states may be of interest for optically controlling the input for all-spin information transfer along spin chains [63–65], or to connect and to switch molecular spin qubit candidates [66, 67].

6 Acknowledgements

References

[1] J. M. Herrera, V. Marvaud, M. Verdaguer, J. Marrot, M. Kalisz, C. Mathoniere, *Angew. Chem.* **2004,** *116,* 5584–5587.

[2] T. Korzeniak, R. Jankowski, M. Kozieł, D. Pinkowicz, B. Sieklucka, *Inorg. Chem.* **2017,** *56,* 12914–12919.

[3] O. Stefanczyk, R. Pełka, A. M. Majcher, C. Mathonière, B. Sieklucka, *Inorg. Chem.* **2018,** *57,* 8137–8145.

[4] B. W. Stein, C. R. Tichnell, J. Chen, D. A. Shultz, M. L. Kirk, *J. Am. Chem. Soc.* **2018,** *140,* 2221–2228.

[5] F. Volatron, D. Heurtaux, L. Catala, C. Mathonière, A. Gloter, O. Stéphan, D. Repetto, M. Clemente-León, E. Coronado, T. Mallah, *Chem. Commun.* **2011,** *47,* 1985–1987.

[6] L. Trinh, *et al. Inorg. Chem.* **2020,** *59,* 13153–13161.

[7] D. A. Bussian, S. A. Crooker, M. Yin, M. Brynda, A. L. Efros, V. I. Klimov, *Nat. Mater.* **2009,** *8,* 35–40.

[8] L. Biadala, *et al. Nat. Nanotechnol.* **2017,** *12,* 569.

[9] S. Lorenz, C. S. Erickson, M. Riesner, D. R. Gamelin, R. Fainblat, G. Bacher, *Nano Lett.* **2020,** *20,* 1896–1906.

[10] B. Náfrádi, P. Szirmai, M. Spina, H. Lee, O. Yazyev, A. Arakcheeva, D. Chernyshov, M. Gibert, L. Forró, E. Horváth, *Nat. Commun.* **2016,** *7,* 1–8.

[11] A. Kirilyuk, A. V. Kimel, T. Rasing, *Rev. Mod. Phys.* **2010,** *82,* 2731.

[12] R. Mikhaylovskiy, E. Hendry, A. Secchi, J. H. Mentink, M. Eckstein, A. Wu, R. Pisarev, V. Kruglyak, M. Katsnelson, T. Rasing, A. Kimel, *Nat. Commun.* **2015,** *6,* 1–9.

[13] T. Li, A. Patz, L. Mouchliadis, J. Yan, T. A. Lograsso, I. E. Perakis, J. Wang, *Nature* **2013,** *496,* 69–73.

[14] J. N. Nelson, J. Zhang, J. Zhou, B. K. Rugg, M. D. Krzyaniak, M. R. Wasielewski, *J. Chem. Phys.* **2020,** *152,* 014503.

[15] S. von Kugelgen, M. D. Krzyaniak, M. Gu, D. Puggioni, J. M. Rondinelli, M. R. Wasielewski, D. E. Freedman, *J. Am. Chem. Soc.* **2021,** .

[16] H. Mao, R. M. Young, M. D. Krzyaniak, M. R. Wasielewski, *J. Phys. Chem. Lett.* **2021,** *12,* 2213–2218.

[17] Rodríguez-Fortea, Antonio and Alemany, Pere and Alvarez, Santiago and Ruiz, Eliseo, *Chem. Eur. J.* **2001,** *7,* 627–637.

[18] T. Steenbock, C. Herrmann, *J. Comput. Chem.* **2018,** *39,* 81–92.

[19] S. Puhl, T. Steenbock, C. Herrmann, J. Heck, *Angew. Chem. Int. Ed.* **2020,** *59,* 2407–2413.

[20] J. C. Colin, T. Mallah, Y. Journaux, F. Lloret, M. Julve, C. Bois, *Inorg. Chem.* **1996,** *35,* 4170–4176.

[21] D. S. Marlin, E. Bill, T. Weyhermüller, E. Bothe, K. Wieghardt, *J. Am. Chem. Soc.* **2005,** *127,* 6095–6108.

[22] E. T. Chernick, Q. Mi, R. F. Kelley, E. A. Weiss, B. A. Jones, T. J. Marks, M. A. Ratner, M. R. Wasielewski, *J. Am. Chem. Soc.* **2006,** *128,* 4356–4364.

[23] M. L. Kirk, D. A. Shultz, R. D. Schmidt, D. Habel-Rodriguez, H. Lee, J. Lee, *J. Am. Chem. Soc.* **2009,** *131,* 18304–18313.

[24] B. K. Rugg, M. D. Krzyaniak, B. T. Phelan, M. A. Ratner, R. M. Young, M. R. Wasielewski, *Nat. Chem.* **2019,** *11,* 981–986.

[25] H. Guo, *et al. Nat. Mater.* **2019,** *18,* 977–984.

[26] M. L. Kirk, D. A. Shultz, D. Habel-Rodriguez, R. D. Schmidt, U. Sullivan, *J. Phys. Chem. B* **2010,** *114,* 14712–14716.

[27] M. L. Kirk, D. A. Shultz, E. C. Depperman, D. Habel-Rodriguez, R. D. Schmidt, *J. Am. Chem. Soc.* **2012,** *134,* 7812–7819.

[28] M. L. Kirk, D. A. Shultz, D. E. Stasiw, G. F. Lewis, G. Wang, C. L. Brannen, R. D. Sommer, P. D. Boyle, *J. Am. Chem. Soc.* **2013,** *135,* 17144–17154.

[29] T. Steenbock, D. A. Shultz, M. L. Kirk, C. Herrmann, *J. Phys. Chem. A* **2017,** *121,* 216–225.

[30] M. L. Kirk, D. A. Shultz, J. Chen, P. Hewitt, D. Daley, S. Paudel, A. van Der Est, *J. Am. Chem. Soc.* **2021,** *143,* 10519–10523.

[31] M. L. Kirk, D. A. Shultz, P. Hewitt, D. E. Stasiw, J. Chen, A. van der Est, *Chem. Sci.* **2021,** .

[32] A. Bencini, D. Gatteschi, *EPR of exchange coupled systems;* Dover Publications Inc.: Mineola, New York, 2012.

[33] S. Grimme, *J. Chem. Phys.* **2013,** *138,* 244104.

[34] C. Bannwarth, S. Grimme, *Comput. Theor. Chem.* **2014,** *1040,* 45–53.

[35] M. de Wergifosse, C. Bannwarth, S. Grimme, *J. Phys. Chem. A* **2019,** *123,* 5815–5825.

[36] E. Runge, E. K. U. Gross, *Phys. Rev. Lett.* **1984,** *52,* 997–1000.

[37] M. Marques, A. Rubio, E. K. Gross, K. Burke, F. Nogueira, C. A. Ullrich, *Time-dependent density functional theory;* volume 706 Springer Science & Business Media: 2006.

[38] C. A. Ullrich, *Time-dependent density-functional theory: concepts and applications;* OUP Oxford: 2011.

[39] C. D. Sherrill, H. F. Schaefer III, *Adv. Quantum Chem.* **1999,** *34,* 143–269.

[40] C. J. Cramer, *Essentials of computational chemistry: theories and models;* John Wiley & Sons: 2013.

[41] L. Noodleman, *J. Chem. Phys.* **1981,** *74,* 5737–5743.

[42] C. R. Jacob, M. Reiher, *Int. J. Quantum Chemistry* **2012,** *112,* 3661–3684.

[43] J. Brüggemann, C. R. Jacob, *Faraday Discuss.* **2020,** *224,* 56–78.

[44] T. Yanai, D. P. Tew, N. C. Handy, *Chem. Phys. Lett.* **2004,** *393,* 51–57.

[45] F. Weigend, *Phys. Chem. Chem. Phys.* **2006,** *8,* 1057–1065.

[46] F. Neese, *J. Phys. Chem. Solids* **2004,** *65,* 781–785.

[47] P.-O. Löwdin, *J. Chem. Phys.* **1950,** *18,* 365–375.

[48] A. E. Clark, E. R. Davidson, *J. Chem. Phys.* **2001,** *115,* 7382–7392.

[49] M. Deffner, L. Gross, T. Steenbock, B. A. Voigt, G. C. Solomon, C. Herrmann, "ARTAIOS - a transport code for postprocessing quantum chemical electronic structure calculations, available from https://www.chemie.uni-hamburg.de/ac/herrmann/software/index.html", 2009-2017.

[50] C. Herrmann, M. Reiher, B. A. Hess, *J. Chem. Phys.* **2005,** *122,* 034102.

[51] E. Ruiz, A. Rodríguez-Fortea, J. Cano, S. Alvarez, P. Alemany, *J. Comput. Chem.* **2003,** *24,* 982–989.

[52] "TURBOMOLE V7.4.1 2019, a development of University of Karlsruhe and-Forschungszentrum Karlsruhe GmbH, 1989-2007,TURBOMOLE GmbH, since 2007; available from
http://www.turbomole.com.", .

[53] P. A. M. Dirac, *Proc. Royal Soc. (London) A* **1929,** *123,* 714–733.

[54] J. C. Slater, *Phys. Rev.* **1951,** *81,* 385.

[55] J. P. Perdew, Y. Wang, *Phys. Rev. B* **1992,** *45,* 13244.

[56] J. P. Perdew, K. Burke, M. Ernzerhof, *Phys. Rev. Lett.* **1996,** *77,* 3865.

[57] R. Kobayashi, R. D. Amos, *Chem. Phys. Lett.* **2006,** *420,* 106–109.

[58] S. Shil, C. Herrmann, *J. Computat. Chem.* **2018,** *39,* 780–787.

[59] T. Risthaus, A. Hansen, S. Grimme, *Phys. Chem. Chem. Phys.* **2014,** *16,* 14408–14419.

[60] T. Steenbock, J. Tasche, A. I. Lichtenstein, C. Herrmann, *Journal of chemical theory and computation* **2015,** *11,* 5651–5664.

[61] J. B. Chapman, P.-W. Ma, S. L. Dudarev, *Phys. Rev. B* **2020,** *102,* 224106.

[62] W. Pfäffle, D. Antonov, J. Wrachtrup, G. Bester, *Phys. Rev. B* **2021,** *104,* 104105.

[63] A. A. Khajetoorians, J. Wiebe, B. Chilian, R. Wiesendanger, *Science* **2011,** *332,* 1062–1064.

[64] A. DiLullo, S.-H. Chang, N. Baadji, K. Clark, J.-P. Klockner, M.-H. Prosenc, S. Sanvito, R. Wiesendanger, G. Hoffmann, S.-W. Hla, *Nano Lett.* **2012,** *12,* 3174–3179.

[65] M. Bazarnik, B. Bugenhagen, M. Elsebach, E. Sierda, A. Frank, M. H. Prosenc, R. Wiesendanger, *Nano Lett.* **2016,** *16,* 577–582.

[66] C. Bonizzoni, A. Ghirri, F. Santanni, M. Atzori, L. Sorace, R. Sessoli, M. Affronte, *npj Quantum Inf.* **2020,** *6,* 1–7.

[67] M. Rubín-Osanz, *et al. Chem. Sci.* **2021,** *12,* 5123–5133.